

Research Article

Influence of vegetation index to the rainfall intensity in Pasuruan Area, East Java Province, Indonesia

Agus Suharyanto*

Civil Engineering Department, Faculty of Engineering, Universitas Brawijaya, Malang, Indonesia

Alwafi Pujiraharjo

Civil Engineering Department, Faculty of Engineering, Universitas Brawijaya, Malang, Indonesia

M. Taufik Iqbal

Doctorate Student of Civil Engineering Department, Faculty of Engineering, Universitas Brawijaya, Malang, Indonesia

*Corresponding author. E-mail: agus.s@ub.ac.id

Article Info

<https://doi.org/10.31018/jans.v16i1.5316>

Received: December 10, 2023

Revised: February 4, 2024

Accepted: February 15, 2024

How to Cite

Suharyanto, A. *et al.* (2024). Influence of vegetation index to the rainfall intensity in Pasuruan Area, East Java Province, Indonesia. *Journal of Applied and Natural Science*, 16(1), 251 - 262. <https://doi.org/10.31018/jans.v16i1.5316>

Abstract

An increase in population increases the rate of urbanization. This results in changes in land cover from vegetation to artificial material. As a result, much of the land surface reflects the sun's energy. Consequently, this increases the surface temperature of the land. An increase in land surface temperature (LST) will increase the intensity of rainfall. Therefore, the present study aimed to investigate the relationship between the increase in LST and rainfall intensity. Changes in land cover can be detected by normalized difference vegetation index (NDVI) and normalized difference built-up index (NDBI) parameters. Landsat satellite imagery was used to detect NDVI, NDBI, and LST. Image processing was done for imageries scanned in 1995, 2015, 2017, and 2021. Two areas in the East Java Province of Indonesia, namely Malang City and Pasuruan Area, were selected. The daily rainfall intensity data were collected from related rainfall stations in the same year. The Mononobe method was applied to analyze hourly and minute rainfall intensity. IDF curves were drawn from the analyzed results. The relationship between both parameters was analyzed by comparing the LST and hourly rainfall intensity from the IDF curve. The studied results showed that the maximum temperature increase from 1995 to 2021 for the Malang City and Pasuruan Area was 2.6^o C and 7.6^o C, respectively. For rain, the maximum rainfall intensity increased by 58 mm for Malang City and 18 mm for the Pasuruan Area. LST and rainfall intensity change trends of the two areas had a positive coefficient of regression. The findings can be used to predict the rainfall intensity and floods based on the LST data.

Keywords: Built-up index, Intensity-duration-frequency curve, Land surface temperature (LST), Normalized difference vegetation index (NDVI), Rainfall intensity

INTRODUCTION

Recently, the global climate is changing very fast. One of the phenomena of global climate change is global warming. This phenomenon is affected by the increase in LST. Increasing LST is caused by several reasons, among them is caused by land use and land cover (LULC) change (Yeneneh *et al.*, 2022 and; Prasetya *et al.*, 2020). In general, LULC change is indicated by the change of land covered by vegetation to land covered by manmade materials such as concrete, asphalt, and other impervious materials. The land covered by concrete can be shown as land covered by parking lot areas, roads, buildings, and other civil structures. Besides

that, the land covered by asphalt can be shown as land covered by roads, parking lots, and other civil structures.

Consequently, the sunlight will be emitted and reflected directly by manmade materials. The emitted and reflected sunlight energy will increase the air temperature (Fu *et al.*, 2020; Martel *et al.*, 2021). Recently, this phenomenon has happened a lot in urban areas. Based on the worldwide population growth, which is high, urbanization is growing rapidly (Satterthwaite, 2019). Therefore, urbanization has caused an increase in the LST, especially in urbanized areas (Imran *et al.*, 2021). An increase in LST will reduce air's relative humidity (RH). Consequently, the evaporation will increase and will be

caused by the formation of clouds that multiply quickly (Roelofs and Kamphuis, 2019). This natural process affects the rainfall characteristics. The rainfall characteristics can be described by a hyetograph and intensity-duration-frequency (IDF) graph (Sun *et al.*, 2019). Satellite remote sensing data is very useful to analyze the LULC and LST changes (Kumar *et al.*, 2018 and Faisal *et al.*, 2021). Normally, LULC change is analyzed using visible wave bands, and LST change is analyzed using thermal bands. Both bands are available in Landsat data with sensor Thematic Mapper (TM), Enhanced Thematic Mapper plus (ETM+), and Operational Land Imager (OLI) (Mansourmoghaddam *et al.*, 2023). Consequently, Landsat imagery can be used to analyze the LULC and LST changes. Meanwhile, one indicator of LULC change that is often used is NDVI. (Husain *et al.*, 2023).

Usually, rainfall data is represented by the minimum, average, and maximum rainfall intensity recorded at the rainfall station. In Indonesia, the rainfall data is generally observed in daily rainfall. Usually, the hourly rainfall intensity data is used to analyze the surface runoff discharge. To change the daily to hourly rainfall intensity data, one of the most popular methods used is the Mononobe method (Suwarno *et al.*, 2021). Hourly rainfall intensity and minute rainfall intensity can be analyzed using the Mononobe method. Hourly rainfall intensity is commonly used to analyze rainfall characteristics. On the other hand, rainfall characteristics represented by the IDF curve with a certain rainfall duration are detailed enough to show the rainfall characteristics.

The IDF curve can be generated from the average daily rainfall intensity using the Mononobe method (Faradiba, 2021). The average rainfall intensity is analyzed using the Thiessen polygon method (Song and Park, 2021). As mentioned above, LULC change affects the change in NDVI. NDVI change affects LST, and LST change affects rainfall characteristics. Therefore, this research investigates the effect of LST change caused by LULC change on rainfall characteristics. One method to show changes in rainfall characteristics is the IDF curve. The IDF method shows the rainfall intensity characteristics in hourly to minutes. This research is important because the rain pattern has been irregular lately and sometimes out of season (Murthy and Kumar, 2022). It is necessary to conduct this research to know the reason for this phenomenon. The present study aimed to determine the relationship between LST and rainfall intensity by comparing trends of both parameters from 1995 to 2021 and to know the increase in LST and rainfall intensity of the study area during this period.

MATERIALS AND METHODS

Study area

East Java Province: Malang City and Pasuruan City, were used as research areas because Malang City is located in a hilly area, and Pasuruan City is located in a flat area near a beach. Both cities have rapid growth populations; therefore urbanization rate is high. Malang City's population in 2021 is estimated to be 844,933, with a population growth of 0.28% (BPS-SMM, 2022).

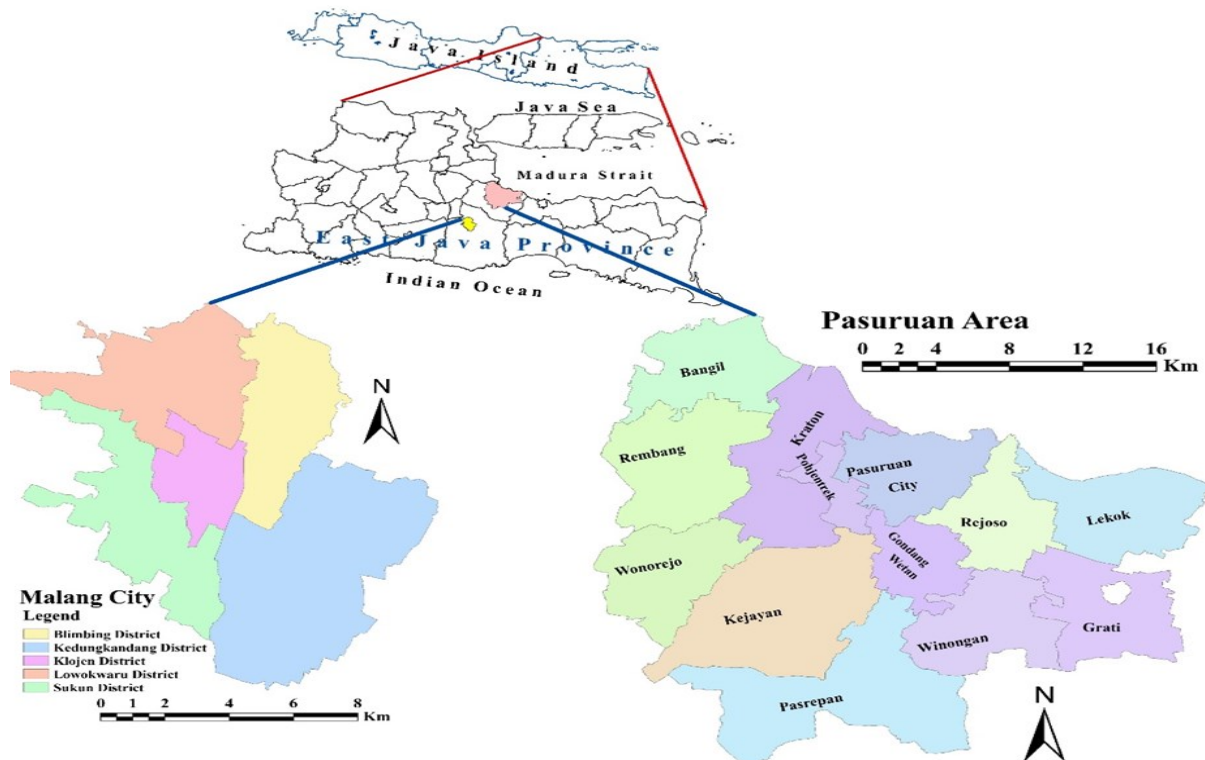


Fig. 1. Map showing studied area (Malang City and Pasuruan Area)

The area of Malang City is 110.06 km² with an elevation of 527 m above sea level. Geographically, the location of Malang City is between 112.06° - 112.07° E and 7.06° - 8.02° S. Population of Pasuruan City in 2021 is 209,528, with a population growth of 0.55% (BPS-SPR, 2022). The area of Pasuruan City is 35.29 km² with an elevation of 4 m above sea level. It is located between 112°45'-112°55' and 7°35' - 7°45' E. Because the area of Pasuruan City was minimal, the boundary of the research area for Pasuruan City was extended to the surrounding area and named Pasuruan Area with a total area equal to 612.1 km². Thus, Malang City represents a city in the mountains and the Pasuruan Area, a city on the coast (Fig. 1).

Data used

The imageries scanned by Landsat satellite were used. The imageries with paths and rows 116/065 and 116/066, which covered Malang City and Pasuruan Area, were generated. The imageries scanned by TM in 1995 and OLI in 2015, 2017, 2019, and 2021 were downloaded from the United States Geological Survey website (USGS, 2019). The images with cloud coverage that covered less than 10% were selected (Table 1).

The rainfall data at the research areas were collected for the same years. The daily rainfall intensity data was collected for each rainfall station based on the data available. There were three rainfall stations in Malang City and 13 in Pasuruan Area. The names and locations of rainfall stations for both research areas are shown in Fig. 2. The rainfall data in Malang City was collected from Dinas Pengairan (Water Resources Agency) East Java Province and rainfall data in Pasuruan Area was collected from Dinas Sumber Daya Air, Cipta Karya, dan Tata Ruang Kabupaten Pasuruan (Water Resources, Human Settlement, and Spatial Planning Agency Pasuruan Regency) in East Java Province.

Research methods

The satellite imageries and rainfall data were collected. The radiometric and geometric correction was done for imagery data. A Universal Transverse Mercator (UTM) coordinate system was used for coordinate reference. NDVI, NDBI, and LST were analyzed from the corrected imageries using the appropriate method. Finally, the NDVI, NDBI, and LST data of the research areas were acquired. The relationship between NDVI-NDBI, NDVI-LST, and NDBI-LST was shown by drawing the curves. This analysis found each research area's minimum, average, and maximum LST in 1995, 2015, 2017, and 2021.

Daily rainfall data was collected from each rainfall station in each research area in the same year as for the imagery data. The maximum rainfall intensity of each

year from each station was selected. The Thiessen polygon method was used to analyze the average rainfall intensity in each research area. Using the Mononobe method, the average daily rainfall intensity was changed to hourly and minute rainfall intensity. The IDF curve was drawn from this data with the X axis as time and the Y axis as rainfall intensity. The relationship between the change in LST and the change in rainfall characteristics was determined by comparing the LST data and IDF data. The curve showing the LST change and rainfall intensity change in each year was drawn. The research method used in this study is shown diagrammatically in Fig. 3.

Image processing

Currently, many artificial satellites are orbiting the earth to record the condition of the earth's surface. Among them is the Landsat satellite jointly programmed by NASA and USGS. The first satellite (Landsat 1) was launched on 23 July 1972 and the last (Landsat 9) was launched on 27 September 2021. Landsats 1 to 3 carried out Multi-Spectral Scanner (MSS) sensor, Landsats 4 to 5 carried out TM scanner, Landsat 6 to 7 carried out ETM+ sensor, and Landsats 8 to 9 carried out OLI (including Thermal InfraRed Sensor-TIRS) scanners. The imageries scanned by TM, ETM+, and OLI were used. There were 7 bands for Landsat TM, 8 for Landsat ETM+, and 11 for Landsat OLI. The image analysis was made using the Geographic Information System (GIS) software used.

One of the important parameters to analyze LULC change is NDVI. This parameter was analyzed using Landsat data. The NDVI was calculated based on the ratio between visible to near-infrared (NIR) light absorbed and reflected by the plant. The formula to calculate NDVI is shown in Eq. 1 (Pei *et al.*, 2021). For Landsat TM and ETM+, NIR and Red are represented by band 4 and band 3, respectively. NDVI for Landsat OLI NIR and Red are represented by band 5 and band 4, respectively. The value of NDVI is from -1 to +1. From -1 to 0, it represents land that is not covered by vegetation. NDVI greater than 0 indicates that the land is covered by vegetation. Plus one indicated that the land was 100% covered by vegetation and smaller than one such land was covered with less than 100% vegetation.

$$NDVI = \frac{NIR - Red}{NIR + Red}$$

Eq. 1

The change of NDVI indicates LULC change. Decreasing NDVI increases the manmade materials covering the land, especially in an urbanized area. The increase of manmade materials covering the land was detected by satellite data using the NDBI method. Short wavelength infrared (SWIR) more reflected manmade materials until bare soil than NIR. The water body does not reflect on the Infrared spectrum and in NDVI indicated

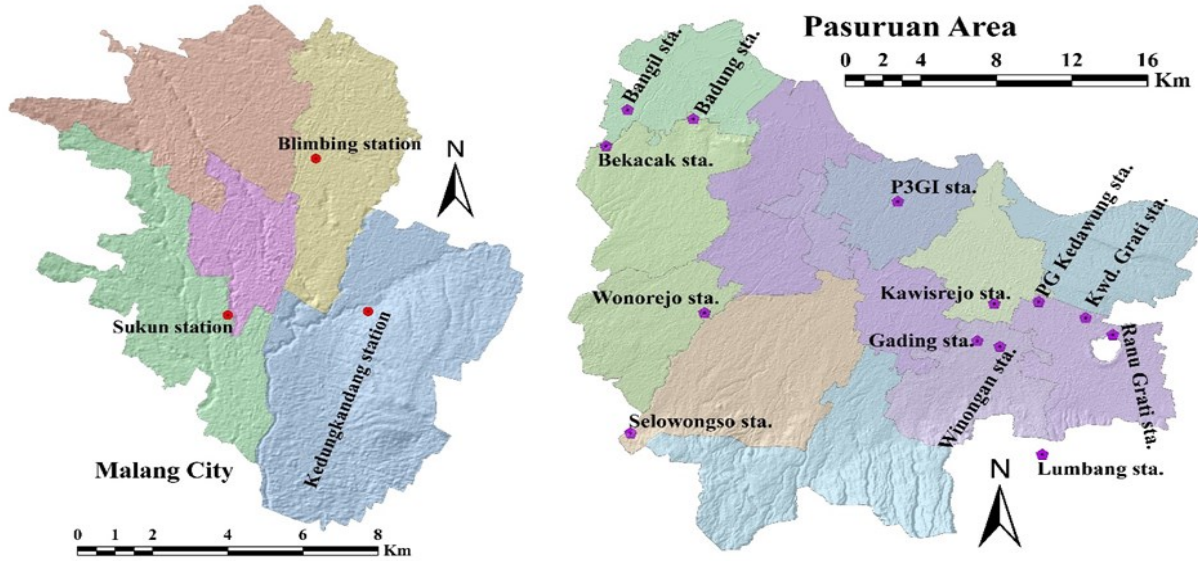


Fig. 2. Rainfall station in the studied area (Malang City and Pasuruan Area)

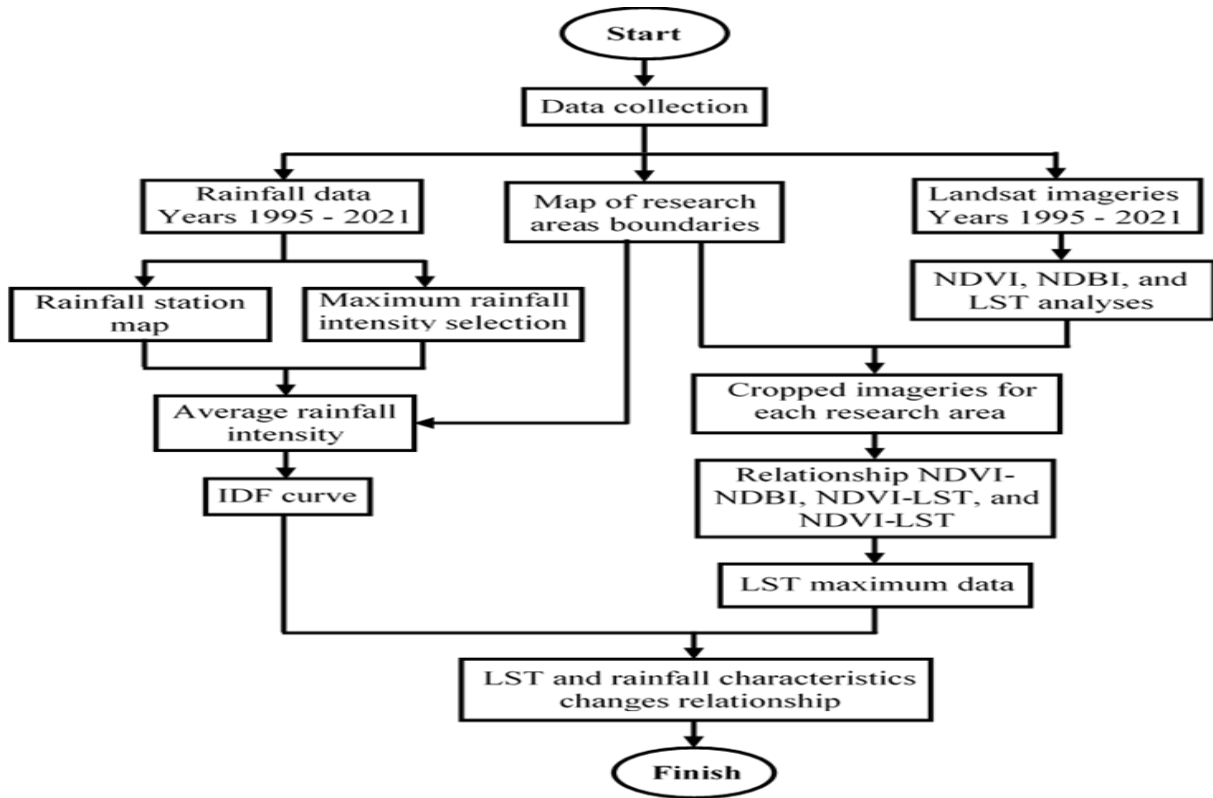


Fig. 3. Flow diagram of the research methodology

by -1 to 0 values. The formula used to calculate the NDBI is shown in Eq. 2 (Orieschnig *et al.*, 2021). The imageries of Landsat TM and ETM+, band 5, and band 4 represent SWIR and NIR. Landsat OLI imageries for SWIR and NIR represent band 6 and 5. The value of NDBI is from -1 to +1. The value -1 to 0 represent the water bodies and higher values represent manmade materials or built-up area.

$$NDBI = \frac{SWIR - NIR}{SWIR + NIR}$$

Eq. 2

A decrease in NDVI will increase NDBI. This phenomenon is common in urban areas. This event will increase LST and its occurrence can be detected with satellite imagery data. The thermal band is commonly used for evaluating the LST. For Landsat TM and ETM+, band 6 was used to evaluate the LST. For Landsat OLI, band 10 or 11 (TIRS band) is used to evaluate the LST. For Landsat TM and ETM+, Eq. 3 - 5 are used to evaluate the LST (Attiah *et al.*, 2023). Eq. 3 to calculate the temperature of the satellite sensor (brightness radiance).

LST in Kelvin unit is calculated with Eq. 4. Finally, LST in Celsius unit is calculated by Eq. 5. To evaluate the LST from Landsat OLI imagery, Eq. 6 - 10 are used (Sekertekin and Bonafoni, 2020). The maximum LST value of each research area in each year is used to analyze the effect of LST change on rainfall characteristics.

$$L_{\lambda} = \frac{L_{max} - L_{min} * (DN - QCAL_{min}) + L_{min}}{QCAL_{max} - QCAL_{min}} \quad \text{Eq. 3}$$

Where L_{λ} is the Top of Atmospheric (TOA) radiance at the sensor's aperture in $W/(m^2sr \mu m)$, $QCAL_{max}$ and $QCAL_{min}$ are the highest and the lowest points of the range of rescaled radiance in digital number (DN), L_{min} and L_{max} are the TOA radiances that were scaled to $QCAL_{min}$ and $QCAL_{max}$ in $W/(m^2sr\mu m)$

$$T = \frac{K_2}{\ln(K_1 / L_{\lambda} + 1)} \quad \text{Eq. 4}$$

$$T_c = T - 273.15 \quad \text{Eq. 5}$$

Where T is the effective at-satellite brightness temperature in Kelvin, $K_1 = 607.76$ ($W/m^2sr\mu m$), $K_2 = 1,260.56$ (Kelvin) were calibration constants, T is the temperature in Kelvin, and T_c is the temperature in Celsius.

$$TOA = M_L * DN + A_L \quad \text{Eq. 6}$$

Where M_L is the radiance multiplicative scaling factor (Radiance_Mult_Band_10 or 11) obtained from the MTL file on the Landsat data, A_L is the radiance additive scaling factor (Radiance_Add_Band_10 or 11) obtained from the MTL file on the Landsat data, and DN is the digital value of Band 10 or 11.

$$T_c = \frac{K_2}{\ln(K_1 / L_{\lambda} + 1)} - 273.15 \quad \text{Eq. 7}$$

Here, L_{λ} is calculated using Eq. 3.

$$PV = \left(\frac{NDVI - NDVI_{min}}{NDVI_{max} - NDVI_{min}} \right) \quad \text{Eq. 8}$$

Where PV is proportional vegetation calculated using the NDVI value, NDVI is DN of NDVI.

$$E = 0.004 * PV + 0.986 \quad \text{Eq. 9}$$

Here, E is error correction.

$$LST = \frac{T_c}{\{1 + [(DN * T_c / \rho) * \ln E]\}} \quad \text{Eq. 10}$$

Where, DN is the digital number of Band 10 (DN is the wavelength of emitted radiance), $\rho = 14,380$ ($\rho = h * c / \sigma$ (1.438×10^{-2} mK)), T_c is the brightness temperature, σ is the Boltzmann constant (1.38×10^{-23} J/K), h is the Planck constant (6.626×10^{-34} Js), and c is the velocity of light (2.998×10^8 m/s).

Extraction of Intensity-Duration-Frequency Curve

There were five steps to evaluate the IDF curve. The first step was to select the maximum daily rainfall intensity each year for each rainfall station. The second step was to calculate the average daily rainfall intensity each year for each research area using the Thiessen polygon method. The third step calculated the hourly and minute rainfall intensity using the Mononobe method. The fourth step drew the IDF curve with X-axis as time and Y-axis as rainfall intensity. As a comparison, the rainfall intensity with several return periods was also evaluated. The statistical method was used to evaluate the rainfall intensity with several return periods (Murthy and Kumar, 2022; Liu et al., 2023). Finally, the IDF curve with several hourly and minute rainfall intensities was drawn. The Thiessen polygon of Malang City is shown in Fig. 4. There were three rainfall stations in Malang City. The steps for drawing Thiessen polygons were as follows. The first was by drawing a line connecting each rainfall station. The second was to divide the line that connects rain stations right in the middle. The third was to make a line perpendicular to the midpoint to the boundary of the area under review. The results of the Malang City and Pasuruan Area Thiessen polygons depiction are mentioned in Fig. 4. The area of influence of each rain station was calculated. The total area of each rainfall station's influence was equal to the area of Malang City. The average rainfall intensity using the Thiessen polygon method is shown in Eq. 11 (Han et al., 2023; Xu et al., 2023).

$$\bar{R} = \frac{A_1 * R_1 + A_2 * R_2 + A_3 + \dots + A_n}{A_1 + A_2 + A_3 + \dots + A_n} \quad \text{Eq. 11}$$

Where \bar{R} is the average rainfall intensity, A_1 is the influence area of rainfall intensity station 1, A_2 is the influence area of rainfall intensity station 2, A_3 is the influence area of rainfall intensity station 3, and A_n is the influence area of rainfall intensity station n.

RESULTS AND DISCUSSION

Change of Normalized Difference Vegetation Index

The Landsat TM scanned in 1995 and OLI scanned in 2015, 2017, 2019, and 2021 were used for analyzing NDVI using Eq. 1. The analyzed results of NDVI in 1995, 2015, and 2021 of research areas are shown in Fig. 5. It was seen that the area of negative, 0-0.1, and 0.1-0.2, represented as red and yellow colors increased from 1995 to 2021 for both Malang City and Pasuruan Area. Hartoyo et al. (2021) mentioned that the NDVI with values negative and 0-0.1 indicated that the area was covered by bare soil, artificial materials, and water, and 0.1-0.2 indicated that there was no canopy vegetation (grasslands) or senescing crops. Furthermore, Milanović et al. (2019) mentioned that 0.3-0.4 and 0.4-0.5 NDVI classes represent the land covered by mid-low

Table 1. Landsat imageries data of covered research areas

No.	Path/Row	Satellites	Sensors	Scanned dates	Covered areas
1.	118/066	Landsat-5	TM	24 May 1995	Malang City
2.	118/065	Landsat-5	TM	25 June 1995	Pasuruan Area
3.	118/066	Landsat-8	OLI	16 June 2015	Malang City
4.	118/065	Landsat-8	OLI	16 June 2015	Pasuruan Area
5.	118/066	Landsat-8	OLI	5 June 2017	Malang City
6.	118/065	Landsat-8	OLI	09 September 2017	Pasuruan Area
7.	118/066	Landsat-8	OLI	13 July 2019	Malang City
8.	118/065	Landsat-8	OLI	13 July 2019	Pasuruan Area
9.	118/066	Landsat-8	OLI	15 May 2021	Malang City
10.	118/065	Landsat-8	OLI	04 September 2021	Pasuruan Area

Source: USGS website (<https://earthexplorer.usgs.gov/>)

canopy cover, low vigor or low canopy cover, and high vigor. The area of each NDVI class every year for both research areas is shown in Fig. 6. This graph shows that in Malang City, the 0.2-0.3 and 0.3-0.4 NDVI classes had an uptrend and the other classes had a down trend. The area of negative, 0-0.1, and 0.1-0.2 NDVI classes in 1995 was 41.865 km²; in 2021, it was 60.399 km². On the other hand, 0.3-0.4 and 0.4-0.5 NDVI classes representing the land covered by mid-low canopy cover, low vigor or low canopy cover, and high vigor decreased from 1995 to 2021. The area of 0.3-0.4 and 0.4-0.5 classes in 1995 was 36.589 km²; in 2021, it became 26.352 km². The 0.5-0.6 NDVI class area represents dense vegetation of 0 km² in 1995 and only 0.022 km² in 2021. It means no big and dense vegetation in Malang City.

For the Pasuruan Area, the NDVI classes between 0-0.1 and 0.3-0.4 had an upward trend. It meant the vegetation with a low canopy (shrubs and grasslands) was going up. On the other hand, class NDVI between 0.4-0.5 and 0.5-0.6 had a downward trend. Therefore, the vegetation with the middle canopy went down. For NDVI greater than 0.6, it only existed in 1995; after that, it was gone. Since 2015, there has been vegetation with a mid-high canopy in the Pasuruan Area.

Change of Normalized Difference Built-up Index (NDBI)

NDBI has indicated the condition of urbanization activity. Positive NDBI indicated that the area has progressed built-up activity or urban land, and negative NDBI represented non-urban land. The NDBI of Malang City and Pasuruan area generated from Landsat imageries is shown in Fig. 7. The NDBI area increased from 1995 to 2021. Based on the graphs shown in Fig. 8, it was seen that the positive NDBI was going up in Malang City and going down in Pasuruan Area. It meant that urbanization in Malang City had positive progress and steady conditions in Pasuruan Area.

Change of Land Surface Temperature (LST)

LST is represented as the temperature at the land surface area. This temperature was estimated using satellite imagery. The thermal band (TIRS) of TM and OLI sensors were used. With band 6 of Landsat 5 TM as input data and applying Eqs. 3-5 for calculation, the LST of the research area in 1995 was evaluated. The values of L_{max} and L_{min} were equal to 15.303 and 1.23, respectively. K_1 and K_2 were equal to 607.76 and 666.09. Based on the DN of band 6, the $QCAL_{max}$ was equal to 255 and $QCAL_{min}$ was equal to 1. Here the



Fig. 4. Thiessen polygon of Malang City and Pasuruan Area

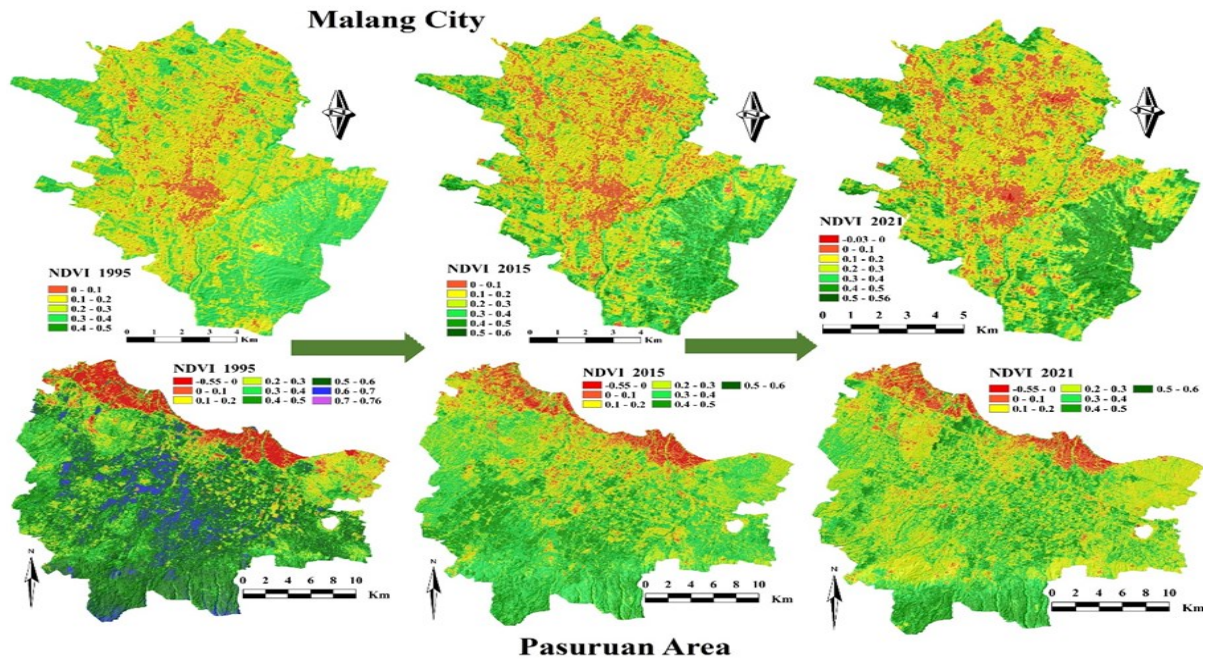


Fig. 5. NDVI images trends of Malang City and Pasuruan Area

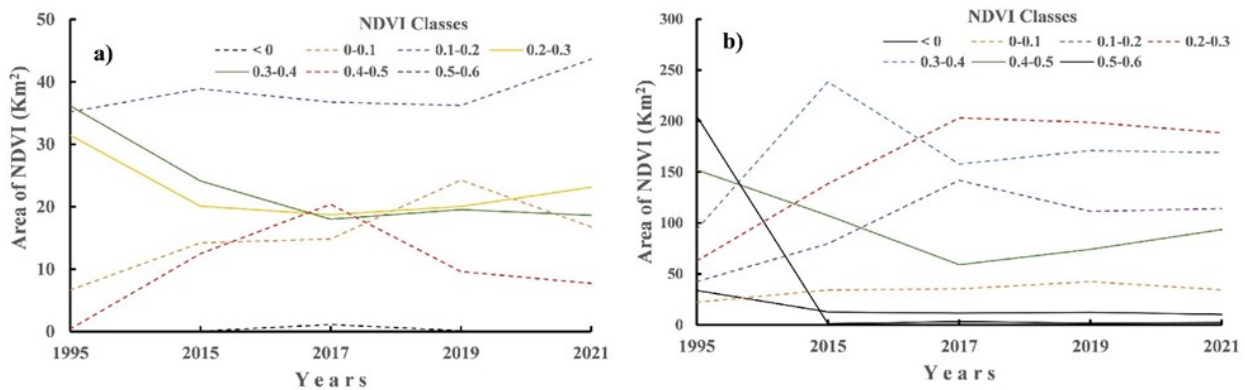


Fig. 6. NDVI trend of the studied areas: a) Malang City and b) Pasuruan Area

LST was equal to the calculation result of T_c . The result of the calculation is shown in Table 2. The LST in the years 2015 to 2021 were calculated using Eqs. 6-10. Band 10 of Landsat 8 OLI was used. Here K_1 and K_2 were equal to 774.89 and 1,321.08, respectively. From the MTL file on the Landsat 8 OLI data used in this research, the M_L and A_L values were equal to 0.0003342 and 0.1, respectively. Based on these parameters and the corresponding DN of satellite imagery data, the LST of all research areas from 2015 to 2021 were analyzed. The results are summarized in Table 2. The change in LST in the study area from 1995 to 2021 is illustrated in the images Fig. 9. It was seen that the LST from 1995 to 2021 had an upward trend. It is shown that the red colour representing the LST with a temperature of more than 30°C increases yearly and is marked with a wider red colour.

Intensity-Duration-Frequency (IDF) curve

The IDF curve shows the characteristics of the rainfall intensity. The daily rainfall intensity of the research ar-

ea was collected from rainfall stations, as shown in Fig. 2. The daily maximum rainfall intensity from 1995 to 2021 for each rainfall station was selected. There were 3 data for Malang City and 13 data for Pasuruan Area for each year. From this data, the average rainfall intensity of the research area was evaluated using the Thiessen polygon method for each year. Based on Fig. 4, the area of influence of each rainfall station was calculated. Using the Mononobe method, the average daily rainfall intensity was calculated for the hourly and minute rainfall. The result of the rainfall intensity evaluation is summarized in Table 3. The IDF curve was drawn and shown in Fig. 10 based on the hourly and minute rainfall intensity.

Land Use Land Cover and rainfall characteristic changes

Based on the analysis result, the LULC change represented by NDVI increased from 1995 to 2021. In contrast, the NDBI fell from 1995 to 2021. In other words, NDVI was inversely proportional to NDBI. The lower the

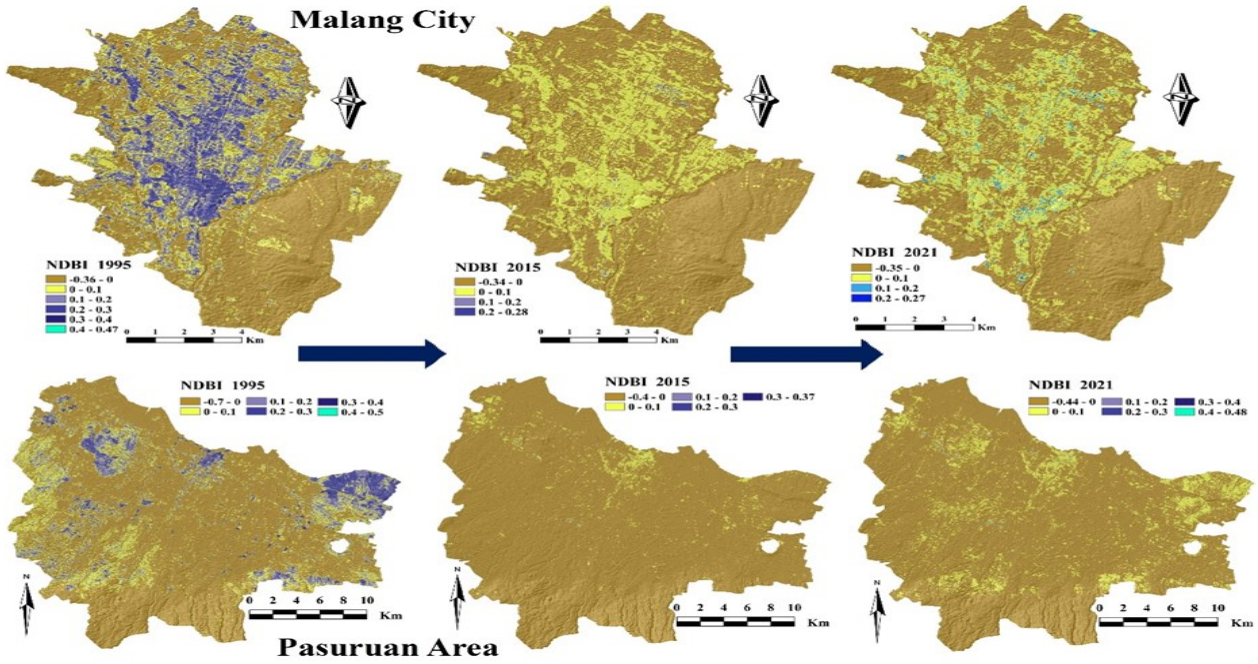


Fig. 7. NDBI images of Malang City and Pasuruan Area

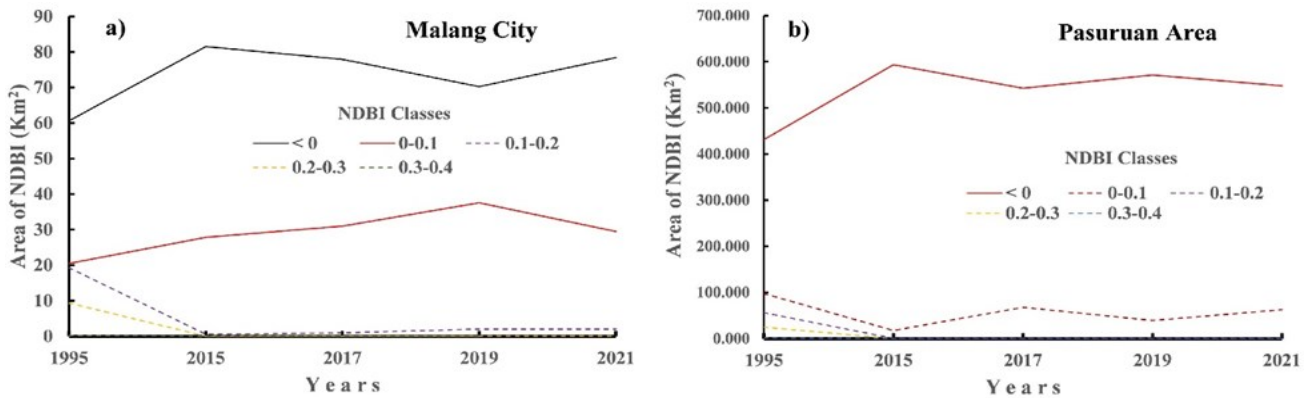


Fig. 8. NDBI trend in the research area: a) Malang City and b) Pasuruan Area

NDVI value, the higher was the NDBI value. This is because land change is from land covered with vegetation (high NDVI) to land covered with manmade materials (high NDBI). The inverse relationship between NDVI and NDBI is agrees with the results of research done by Shahfahad *et al.*, 2020 and Hasan *et al.*, 2022). According to some previous research results, NDVI and LST have an inverse relationship (Guha *et al.*, 2020; Garouani *et al.*, 2021). If the NDVI value is greater, the LST value will decrease. If the NDVI decreases, the normalized difference built-up index (NDBI) will increase. Consequently, LST is directly proportional to NDBI. This means that if the NDBI goes up, LST will also increase (Guha *et al.*, 2020; Meng *et al.*, 2022).

Land covered with vegetation absorbs strongly and emits weak sunlight energy (Dou *et al.*, 2023; Gennaro *et al.*, 2023). On the other hand, land covered with manmade materials will strongly reflect and radiate solar energy. Consequently, the LST will increase if the

NDVI decreases and NDBI increases. In the case of Malang City and Pasuruan Area, the maximum and average LST increased from 1995 to 2021. Therefore, it can be summarized that LST is directly proportional to NDBI and inversely proportional to NDVI. The relationship between LST, NDBI, and NDVI in studied areas from 1995 to 2021 agrees with the research done by the previous researcher (Kaiser *et al.*, 2022 and Kulsum and Moniruzzaman, 2022) in Porto Alegre city, Rio Grande do Sul state, Brazil. An increase in LST decreases the atmosphere's relative humidity (RH) (Lee *et al.*, 2022; Dou *et al.*, 2023). Consequently, if the RH decreases, the soil surface evaporation will increase. As a result of this phenomenon, the formation of clouds becomes denser due to increasing LST. Therefore, the possibility of rain with higher intensity will be more obvious. This phenomenon occurred in the Malang City and Pasuruan Area from 1995 to 2021. The LST and maximum-average rainfall intensity increased from 1995 to 2021. Therefore, it can be summarized

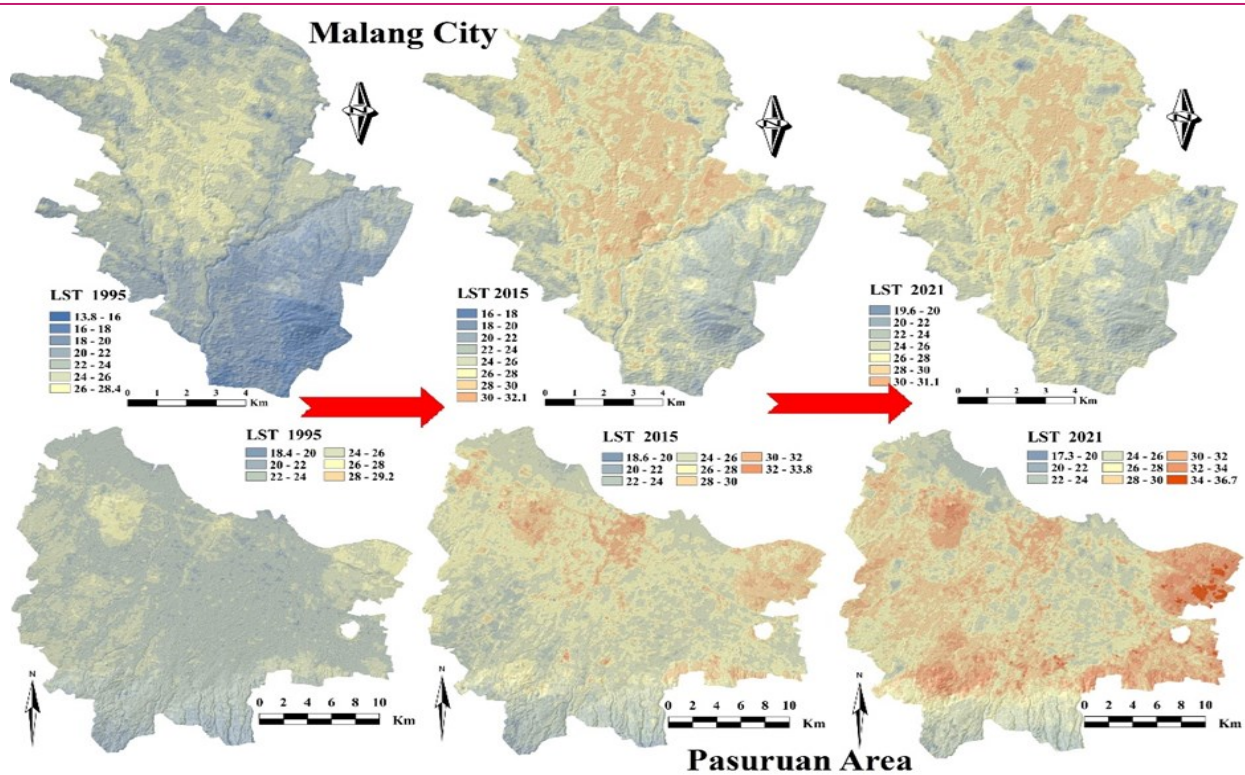


Fig. 9. LST of Malang City and Pasuruan Area

Table 2. LST of studied areas

Research areas	LST (°C)									
	1995		2015		2017		2019		2021	
	Min.	Max.	Min.	Max.	Min.	Max.	Min.	Max.	Min.	Max.
Malang City	13.8	28.4	16	32	21.2	33	19	30.7	19.6	31
Pasuruan Area	18.4	29.2	18.6	33.8	15.2	39.3	17.9	37	17.2	36.8

that LST was directly proportional to rainfall intensity. The regression and correlation method was applied to evaluate the relationship between LST and rainfall intensity changes. The results of regression and correlation analyses have been compared to determine the relationship between LST and rainfall intensity trends from 1995 to 2021.

The hourly rainfall intensity is generally used as input data to evaluate the runoff discharge. Daily rainfall was converted to hourly rainfall to more clearly see changes in rain intensity. Consequently, based on the IDF curves, as shown in Fig. 10, the hourly rainfall data was used to analyze the trend of rainfall intensity from 1995 to 2021. The curves showing the trends of LST and hourly rainfall intensity in the studied areas are shown in Fig. 11. This figure shows that the trend of both LST and rainfall intensity increased year to year. In the case of Malang City, the trend of increasing LST is smaller than the trend of increasing rainfall intensity. The difference in this trend can be seen numerically from the significant differences in the values of the regression and determination coefficients. The coefficients of regression of the LST and rainfall intensity trend are

0.418 and 3.774 and the coefficients of determination are 0.145 and 0.573, respectively. This phenomenon occurs because of the geographical location of Malang City, which is in a mountainous area with an elevation of 527 m above sea level. Consequently, LST will be lower in flat and low areas, with higher rainfall due to the orographic rainfall. For the Pasuruan Area, both LST and rainfall intensity have almost the same increase trends. Numerically, these trends can be shown by the regression and determination coefficients from both regression equations. The coefficients of regression of LST and rainfall intensity trends were 1.827 and 2.829, with coefficients of determination equal to 0.547 and 0.459, respectively. In 2015, some data was contrary to the overall trend. In that year, LST fell, but rainfall intensity rose. This is because the La Nina effect occurred in coastal areas in the East Java Province area in that year (BPS-SJTP, 2020). However, the overall trend for LST and rainfall increased yearly. Because Pasuruan Area is flat and close to the coast, there was no orographic rain effect. Therefore, the trend of rising LST and rainfall intensity becomes the same or in line.

Table 3. Maximum and average rainfall intensity in the studied areas

Research areas	Rainfall Stations	Rainfall intensity (mm/day)									
		1995		2015		2017		2019		2021	
		Max.	Ave.	Max.	Ave.	Max.	Ave.	Max.	Ave.	Max.	Ave.
Malang City	Blimbing	84	70	96	122	104	113	82	115	123	128
	Kedungkandang	92		110		106		135		133	
	Sukun	96		170		132		130		120	
Pasuruan Area	Badung	88	83	77	84	95	93	187	129	123	101
	Bangil	93		98		91		93		102	
	Bekacak	88		135		108		100		93	
	Gading	87		112		110		70		66	
	Kawisrejo	50		87		108		111		117	
	Kwd. Grati	67		62		117		126		85	
	Lumbang	85		98		84		136		71	
	P3GI	87		68		67		100		93	
	PG Kedawung	48		95		116		129		103	
	Ranu Grati	74		75		114		144		89	
Selowongso	87		85		98		70		96		
Winongan	92		77		53		130		130		
Wonorejo	87		67		89		81		98		

Source: Analyzed result (<https://hidrologi.dpuair.jatimprov.go.id/>)

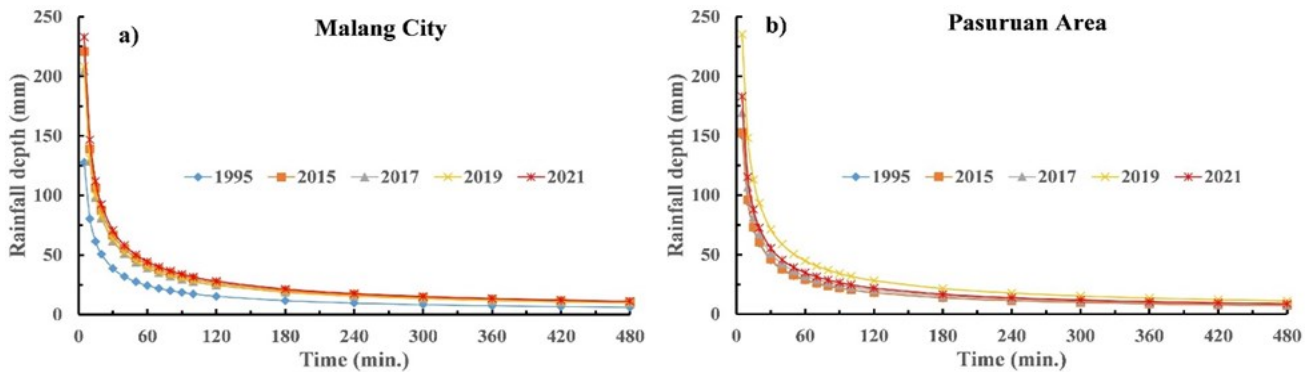


Fig. 10. IDF of research areas: a) Malang City and b) Pasuruan Area

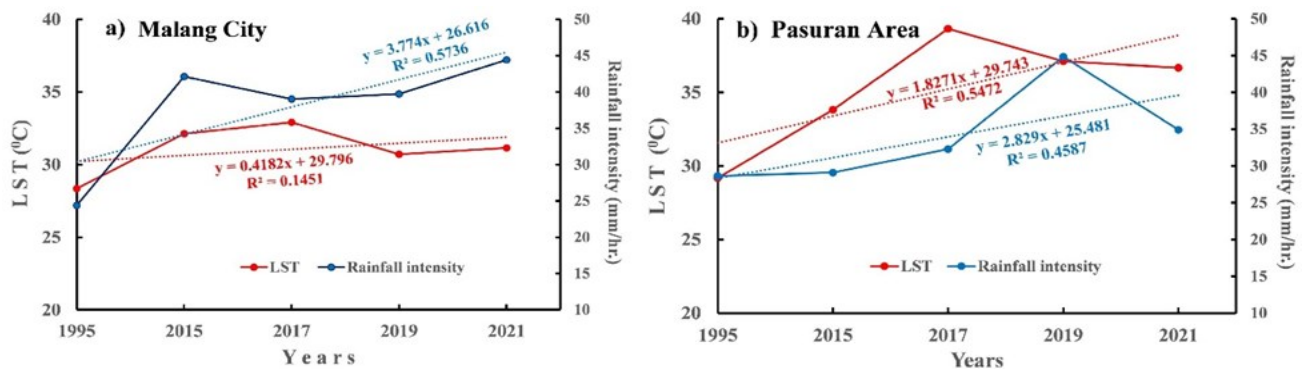


Fig. 11. Trend of LST and rainfall intensity: a) Malang City and b) Pasuruan Area

Conclusion

The present study determined the relationship between LULC changes and changes in NDBI, LST, and rainfall intensity characteristics from 1995 to 2021 in Malang City and Pasuruan Area. NDVI changes indicated LULC changes and the IDF curve represented rainfall

intensity characteristic changes. Landsat imageries scanned by TM and OLI sensors were used. The daily rainfall data was collected for the related research area. From the analyzed result, it was concluded that the NDVI was inversely proportional to NDBI and also to LST. On the other hand, NDBI was directly proportional to LST. There was an upward trend of LST and rainfall

intensity yearly. In mountainous areas represented by Malang City, the increasing trend of LST was higher than the rainfall intensity trend. This happened because the influence of orographic rain in mountainous areas increased the rainfall intensity. In contrast, with an elevation of 527 m above sea level, the LST of Malang City decreased along with its height. Meanwhile, the relationship between LST and rainfall for flat areas close to the coast (Pasuruan Area) had a corresponding upward trend. The trend had the same increasing value for LST and rainfall intensity. The results of this study can be used to predict the amount of rainfall that will fall based on LST data in Malang City and the Pasuruan Area. This will be useful in predicting floods. To increase the accuracy, research needs to be carried out over a wider area, for example, the entire East Java Province, Indonesia.

ACKNOWLEDGEMENTS

The author would like to thank all parties who have assisted in this research. Our special thanks go to Dinas Pengairan East Java Province, Dinas Sumber Daya Air, Cipta Karya, and Tata Ruang Pasuruan Regency for supporting rainfall data. This research was funded by Doktor Lektor Kepala research grant from the Faculty of Engineering Universitas Brawijaya [Vide No. 17/UN10.F07/PN/2022].

Conflict of interests

The authors declare that they have no conflict of interest.

REFERENCES

- Attiah, G., Pour, H. K. & Scott, K. A. (2023). Lake surface temperature retrieved from Landsat satellite series (1984 to 2021) for the North Slave Region. *Earth Syst. Sci. Data*, 15, 1329–1355. <https://doi.org/10.5194/essd-15-1329-2023>.
- BPS-SJTP (2022). Jawa Timur Province in figure. <https://jatim.bps.go.id/publication/2022/02/25/33699f6fcd84e0e2a0ad96f0/provinsi-jawa-timur-dalam-angka-2022.html>.
- BPS-SJTP (2020). Jawa Timur Province in figure. <https://jatim.bps.go.id/publication/2020/05/19/6225e5df323aa13d4fb1e4f4/provinsi-jawa-timur-dalam-angka-2020.html>.
- BPS-SMM (2022). Malang Municipality in figures. <https://malangkota.bps.go.id/publication/2022/02/25/f0956410736a31dde7f7af54/kota-malang-dalam-angka-2022.html>.
- BPS-SPR (2022). Pasuruan Regency in figures. <https://pasuruankab.bps.go.id/publication/2022/02/25/0836f4c232ea044ec9b1f5e5/kabupaten-pasuruan-dalam-angka-2022.html>.
- Dou, J., Grimmond, S, Miao, S., Huang, B., Lei, H. & Liao, M. (2023). Surface energy balance fluxes in a suburban area of Beijing: energy partitioning variability. *Atmos. Chem. Phys.*, 23, 13143–13166. <https://doi.org/10.5194/acp-23-13143-2023>.
- Faisal, A. A., Kafy, A. A., Rakib, A. A., Akter, K. S., Jahir, D. M. A., Sikdar, M. S., Ashrafid, T. J., Mallik, S. & Rahman, M. M. (2021). Assessing and predicting land use/land cover, land surface temperature and urban thermal field variance index using Landsat imagery for Dhaka Metropolitan area. *Environ. Challenges*, 4. <https://doi.org/10.1016/j.envc.2021.100192>.
- Faradiba (2021). Analysis of intensity, duration, and frequency rain daily of Java Island using Mononobe method. *J. Phys. Conf. Ser.*, 1783. <https://doi.org/10.1088/1742-6596/1783/1/012107>.
- Fu, Y., Ma, Y., Zhong, L., Yang, Y., Guo, X., Wang, C., Xu, X., Yang, K., Xu, X., Liu, L., Fan, G., Li, L. & Wang, D. (2020). Land-surface processes and summer-cloud-precipitation characteristics in the Tibetan Plateau and their effects on downstream weather: a review and perspective. *Natl. Sci. Rev.*, 7 (3), 500-515. <https://doi.org/10.1093/nsr/nwz226>.
- Garouani, M. E., Amyay, M., Lahrach, A. & Oulidi, H. J. (2021). Land surface temperature in response to land use/cover change based on remote sensing data and GIS techniques: Application to Saïss Plain Morocco. *J. Ecol. Eng.*, 22(7). <https://doi.org/10.12911/22998993/139065>.
- Gennaro, S., Cerrato, R., Salvatore, M. C., Salzano, R., Salvatori, R., & Baroni, C. (2023). NDVI analysis for monitoring land-cover evolution on selected deglaciated areas in the Gran Paradiso Group (Italian Western Alps). *Remote Sens.*, 15, 3847. <https://doi.org/10.3390/rs15153847>.
- Guha, S., Govil, H. & Diwan, P. (2020). Monitoring LST-NDVI relationship using premonsoon Landsat datasets. *Adv. Meteorol.* <https://doi.org/10.1155/2020/4539684>.
- Guha, S., Govil, H., Gill, N. & Dey, A. (2020). A long-term seasonal analysis on the relationship between LST and NDBI using Landsat data. *Quat. Int.*, 575-576, 249-258. <https://doi.org/10.1016/j.quaint.2020.06.041>.
- Han, Z., Zuo, Q., Wang, C. & Gan, R. (2023). Impacts of climate change on natural runoff in the Yellow River Basin of China during 1961–2020. *Water*, 15, 929. <https://doi.org/10.3390/w15050929>.
- Hartoyo, A. P. P., Sunkar, A., Ramadani, R., Faluthi, S. & Hidayat, S. (2021). Normalized difference vegetation index (NDVI) analysis for vegetation cover in Leuser ecosystem area, Sumatra, Indonesia. *Biodiversitas*, 22, 1160-1171.
- Hasan, M., Hassan, L., Abdullah, Al. M., Abualreesh, M. H., Idris, M. H., & Kamal, A. H. M. (2022). Urban green space mediates spatiotemporal variation in land surface temperature: a case study of an urbanized city, Bangladesh. *Environmental Science and Pollution Research*, 29, 36376–36391. <https://doi.org/10.1007/s11356-021-17480-9>.
- Husain, M.A., Kumar, P. & Gonencgil, B. (2023). Assessment of Spatio-Temporal Land Use/Cover Change and Its Effect on Land Surface Temperature in Lahaul and Spiti, India. *Land*, 12, 1294. <https://doi.org/10.3390/land12071294>.
- Imran, H. M., Hossain, A., Islam, A. K. M. S., Rahman, A., Bhuiyan, M. A. E., Paul, S. & Alam, A. (2021). Impact of land cover changes on land surface temperature and human thermal comfort in Dhaka City of Bangladesh. *Earth*

- Syst. Environ.*, 5, 667-693. <https://doi.org/10.1007/s41748-021-00243-4>.
19. Kaiser, E. A., Rolim, S. B. A., Grondona, A. E. B., Hackmann, C. L., Linn, R. M., Käfer, P. S., Rocha, N. S. & Diaz, L. R. (2022). Spatiotemporal influences of LULC changes on land surface temperature in rapid urbanization area by using Landsat-TM and TIRS images. *Atmosphere*, 13 (3), 460. <https://doi.org/10.3390/atmos13030460>.
 20. Kulsum, U. & Moniruzzaman, M. D. (2022). Exploring the relationship of climate change and land-use dynamics with satellite-derived surface indices and temperature in greater Dhaka, Bangladesh. *J. Earth Syst. Sci.*, 131 (117). <https://doi.org/10.1007/s12040-022-01841-0>.
 21. Kumar, P., Husain, A., Singh, R. B. & Kumar, M. (2018). Impact of land cover change on land surface temperature: a case study of Spiti Valley. *Journal of Mountain Science. J. Mt. Sci.*, 15 (8), 1658-1670. <https://doi.org/10.1007/s11629-018-4902-9>.
 22. Lee, G., Kim, G., Min, G., Kim, M., Jung, S., Hwang, J. & Cho, S. (2022). Vegetation classification in urban areas by combining UAV-based NDVI and thermal infrared image. *Appl. Sci.*, 13, 515. <https://doi.org/10.3390/app13010515>.
 23. Liu, X., Ouyang, C. & Zhou, Y. (2023). A Low-Return-Period Rainfall Intensity Formula for Estimating the Design Return Period of the Combined Interceptor Sewers. *Water Resources Management*, 37, 289–304. <https://doi.org/10.1007/s11269-022-03369-w>.
 24. Mansourmoghaddam, M., Rousta, I., Cabral, P., Ali, A. A., Olafsson, H., Zhang, H. & Krzyszczyk, J. (2023). Investigation and prediction of the Land Use/Land Cover (LU/LC) and Land Surface Temperature (LST) changes for Mashhad City in Iran during 1990–2030. *Atmosphere*, 14, (741). <https://doi.org/10.3390/atmos14040741>.
 25. Martel, J. L., Brissette, F. P., Picher, P. L., Troin, M. & Arsenault, R. (2021). Climate change and rainfall intensity–duration–frequency curves: Overview of science and guidelines for adaptation. *J. Hydrol. Eng.*, 26 (10). [https://doi.org/10.1061/\(ASCE\)HE.1943-5584.0002122](https://doi.org/10.1061/(ASCE)HE.1943-5584.0002122).
 26. Meng, Q., Liu, W., Zhang, L., Allam, M., Bi, Y., Hu, X., Gao, J., Hu D. & Jancsó, T. (2022). Relationships between land surface temperatures and neighboring environment in highly urbanized areas: Seasonal and scale effects analyses of Beijing, China. *Remote Sens.*, 14 (17), 4340. <https://doi.org/10.3390/rs14174340>.
 27. Milanović, M. M., Micić, T., Lukić, T., Nenadović, S. S., Basarin, B., Filipović, D. J., Tomić, M., Samardžić, I., Srdić, Z., Nikolić, G., Ninković, M. M., Sakulski, D. & Ristanović, B. (2019). Application of Landsat-derived NDVI in monitoring and assessment of vegetation cover changes in central Serbia. *Carpathian J. Earth Environ. Sci.*, 14 (1), 119-129. <https://doi.org/10.26471/cjees/2019/014/064>.
 28. Murthy, K. V. N. & Kumar, G. K. (2022). Distribution and Prediction of Monsoon Rainfall in Homogeneous Regions of India: A Stochastic Approach. *Pure Appl. Geophys*, 179, 2577–2590. <https://doi.org/10.1007/s00024-022-03042-8>.
 29. Orieschnig, C. A., Belaud, G., Venot, J. P., Massuel, S. & Ogilvie, A. (2021). Input imagery, classifiers, and cloud computing: Insights from multi-temporal LULC mapping in the Cambodian Mekong Delta. *Eur. J. Remote Sens.*, 54 (1). <https://doi.org/10.1080/22797254.2021.1948356>.
 30. Pei, F., Zhou, Y. & Xia, Y. (2021). Application of Normalized Difference Vegetation Index (NDVI) for the Detection of Extreme Precipitation Change. *Forest*, 12 (5), 594. <https://doi.org/10.3390/f12050594>.
 31. Prasetya, T. A. E., Munawar, Taufik, M. R., Chesok, S., Lim, A. & McNeil, D. (2020). Land surface temperature assessment in Central Sumatra, Indonesia. *Indones. J. Geogr.*, 52 (2). <https://doi.org/10.22146/ijg.51327>.
 32. Roelofs, G. J. & Kamphuis, V. (2019). Cloud processing, cloud evaporation and Angström exponent. *Atmos. Chem. Phys.*, 9, 71-80.
 33. Satterthwaite, D. (2019). The implications of population growth and urbanization for climate change. *Environ. Urbanization*, 21 (2). <https://doi.org/10.1177/0956247809344361>.
 34. Sekertekin, A. & Bonafoni, S. (2020). Land surface temperature retrieval from Landsat 5, 7, and 8 over rural areas: Assessment of different retrieval algorithms and emissivity models and toolbox implementation. *Remote Sens.*, 12 (2), 294. <https://doi.org/10.3390/rs12020294>.
 35. Shahfahad, Kumari, B., Tayyab, M., Ahmed, I. A., Baig, M. R. I., Khan, M. F. & Rahman, A. (2020). Longitudinal study of land surface temperature (LST) using mono- and split-window algorithms and its relationship with NDVI and NDBI over selected metro cities of India. *Arab J Geosci.*, 13, 1040. <https://doi.org/10.1007/s12517-020-06068-1>.
 36. Song, Y. & Park, M. (2021). A Study on the appropriateness of the drought index estimation method using damage data from Gyeongsangnamdo, South Korea. *Atmosphere*, 12 (8), 998. <https://doi.org/10.3390/atmos12080998>.
 37. Sun, Y., Wendi, D., Kim, D. E. & Liang, S. Y. (2019). Deriving intensity–duration–frequency (IDF) curves using downscaled in situ rainfall assimilated with remote sensing data. *Geosci. Lett.*, 6 (17). <https://doi.org/10.1186/s40562-019-0147-x>.
 38. Suwarno, I., Ma'arif, A., Raharja, N. M., Nurjanah, A., Ikhsan, J. & Mutiarin, D. (2021). IoT-based lava flood early warning system with rainfall intensity monitoring and disaster communication technology. *Emerging Sci. J.*, 4. <https://doi.org/10.28991/esj-2021-SP1-011>.
 39. USGS, *Landsat 7 (L7) data users' handbook, version 2*, 122. (2019). United State Geological Survey. <https://www.usgs.gov/media/files/landsat-7-data-users-handbook>.
 40. Xu, Y., Liu, C., Wang, L. & Zou, L. (2023). Exploring the spatial autocorrelation in soil moisture networks: Analysis of the bias from upscaling the Texas Soil Observation Network (TxSON). *Water*, 15, 87. <https://doi.org/10.3390/w15010087>.
 41. Yeneneh, N., Elias, E. & Feyisa, G. L. (2022). Detection of land use/land cover and land surface temperature change in the Suha Watershed, North-Western highlands of Ethiopia. *Environ. Challenges*, 7. <https://doi.org/10.1016/j.envc.2022.100523>.